ADVANCED FUNCTIONAL MATERIALS
www.afm-journal.de

Quantitative In Situ Mechanical Characterization of the Effects of Chemical Functionalization on Individual Carbon Nanofibers

Jiangnan Zhang, Phillip Loya, Cheng Peng, Valery Khabashesku, and Jun Lou**

Carbon nanofibers (CNFs) have been used for applications in composite material for decades because of their unique mechanical, thermal, and electrical properties. Consequently, an in-depth understanding of mechanical properties of individual CNFs, particularly after chemical functionalization, would provide important insight into its effective integration into composite materials. Fluorination and amination of CNFs is achieved and systematic chemical characterizations of functionalized CNFs are performed. An in situ tensile testing method, which combines a simple microfabricated device with a quantitative nanoindenter inside a scanning electron microscope (SEM) chamber, is used to measure mechanical properties of individual pristine, fluorinated, and amino-functionalized CNFs. The nominal CNFs strengths follow the Weibull distribution and the fluorinated CNFs are found to possess higher nominal strength but similar strain when compared with the pristine and amino-functionalized CNFs. SEM fracture surfaces analysis shows that all nanofibers failed in a similar cup-and-cone fashion. Microscopy image sof fluorinated CNFs reveal an unexpected change in the hollow core before and after fiber fracture, which is attributed to the possible effects of fluorination-induced compression on nanofiber surfaces. The results demonstrate the potential of fluorination for improving both the mechanical properties of CNFs and their successful integration into composites.

1. Introduction

The high strength-to-weight ratio combines with superior stiffness have made carbon nanofibers (CNFs) the material of choice for high performance composite structure in aerospace, defense, and other industries.[1–3] The fact that CNFs can be produced in large quantity and at low cost is particularly attractive for these applications compared to carbon nanotubes. However, the challenges associates with CNFs dispersion and poor load transfer between CNFs and matrices, have been a bottleneck for the development of CNFs based composite structures. One popular approach to address these issues and to improve the properties of CNFs based composites is to chemically modify the nanofiber surface with functional groups. Therefore, an in-depth understanding of the structure and mechanical properties of the functionalized CNFs at a single fiber level would be a critical step to improve their integration into different matrices. Nevertheless, the mechanical properties of individual functionalized CNFs have not been systematically explored.

Due to the lack of structural perfection and the existence of a complex hybrid structure,[4,5] it is extremely difficult to obtain theoretical prediction for CNFs strength without extensive simplifications and assumptions.[6] Furthermore, owing to the small sample size as well as the magnitude of the forces and the deformation involved, quantitative mechanical measurements of individual CNFs are considered extremely challenging. The most popular approach to these measurements is atomic force microscope (AFM) based bending test and many attempts have already been made to measure the elastic moduli of CNFs in this manner. The Young's modulus of a suspended CNFs rope was determined to be 400 GPa by Kim et al.[7] Lawrence et al.[8] and Zhang et al.[9] obtained the elastic modulus of individual CNFs to be in the range of 6–207 GPa and the average tensile modulus of single-walled carbon nanotube bundle to be 265 GPa by using the similar technique. Furthermore, Zussman et al.[10] reported the mechanical properties of solid electronspun polyacrylonitrile (PAN)-derived CNFs: the failure stress of CNFs varied from 0.32 to 0.90 GPa and the average Young's modulus was 63 ± 7 GPa. In addition, Inaba et al.[11] found the Young's modulus to be 38–48 GPa for CNFs probes fabricated by the argon ion bombardment of carbon coated silicon cantilever. However, the limitation of AFM based testing, such as poor accuracy and reproducibility, greatly hampers the mechanical measurement of individual CNFs.

Microelectromechanical systems (MEMS) offer a promising class of very small actuators and diagnostic tools for stretching

J. Zhang, P. Loya, C. Peng, Dr. J. Lou
Department of Mechanical Engineering
and Materials Science
Rice University
Houston, TX 77005, USA
E-mail: jlou@rice.edu
Dr. V. Khabashesku
Department of Chemical and Biomolecular Engineering
Cullen College of Engineering
University of Houston
Houston, TX 77204, USA
E-mail:valery@central.uh.edu

DOI: 10.1002/adfm.201200593

nanomaterials under various mechanical and electromechanical loading conditions. The individual pristine, high temperature heat-treated and graphitized/surface oxidized vapor grown carbon nanofibers (VGCNFs) were evaluated for their elastic modulus and tensile strength by Ozkan et al.[12] using a MEMS loading platform. They claimed that the VGCNFs with diameters of the order of 150–300 nm had high tensile strengths between 2.74 GPa and 3.34 GPa, and Young's modulus between 180 GPa and 245 GPa. In addition, with the aid of the same MEMS system, Arshad et al.[13] quantified the average tensile strength and the elastic modulus of the individual solid electrospun PAN-derived CNFs carbonized at 1400 °C to be 3.5 ± 0.6 GPa and 172 ± 40 GPa, which were 6 and 3 times higher than the previous reports,[10,14] respectively. The electrospun CNFs is solid in the inner structure while the functionalized CNFs in this report are mostly hollow.

Herein we report the use of a simple micro-fabricated device that works in conjunction with a quantitative nanoindenter within an SEM chamber to characterize the mechanical properties of pristine, fluorinated and amino-functionalized CNFs. Careful structural characterizations of these CNFs were performed, followed by the quantitative in situ mechanical measurements. These direct tensile strength measurement data obtained from individual CNFs were discussed in the context of different chemical functionalization schemes and modes of fracture as observed in scanning electron microscopy (SEM) and transmission electron microscopy (TEM).

2. Results and Discussion

2.1. Characterizations of Functionalized Carbon Nanofibers

The attenuated total reflectance Fourier transform infrared (ATR-FTIR) spectroscopy provided information on structural nature and vibrational properties of functional groups covalently bonded to CNFs surface (**Figure 1**). In the ATR-FTIR spectrum of fluorinated CNFs (Figure 1a) the highest intensity band at ≈1200 cm^{-1} characterized the stretching modes of C-F and CF_2 groups, while the band at ≈700 cm^{-1} belonged to deformation modes of these groups. The medium intensity band at ≈1560 cm^{-1} was related to activated C=C stretching mode of the CNFs surface. Such spectroscopic "fingerprints" were similar to those observed in fluorinated carbon nanotubes.[15–17] The ATR-FTIR spectrum of amino-functionalized CNFs sample (Figure 1b) showed a broad band centered at ≈3070 cm^{-1} which was crucial for identification of NH and NH_2 groups (N-H stretches). Deformation modes of these groups appeared in this spectrum at ≈1560 and ≈1520 cm^{-1}, as well as twisting mode at ≈714 cm^{-1}. Weaker bands near 2830 cm^{-1} characterized C-H stretches and broad band at ≈1100 cm^{-1} has been associated with the C-C and C-N stretches of the ethylenediamino groups bonded to CNFs surface. In comparison, the FTIR spectrum of pristine CNFs (Figure 1c) did not show a distinct features of surface bonded and IR active groups.

We also compared the results of thermogravimetric analysis (TGA) study of three types of CNFs (see Supporting Information). The complete weight loss of pristine CNFs due to thermal oxidation of CNFs and volatilization of products was observed above 600 °C. For fluorinated CNFs, the weight loss of ≈28% was observed to take place in the temperature range of 250–550 °C. From previous studies of other fluorinated carbon materials, such as graphite and carbon nanotubes, it was known that fluorocarbons eliminated fluorine groups in the form of CF_4 and COF_2 molecules (when air is present). Taking this into account, the weight content of fluorine groups in the CNFs was calculated as ≈24.7%, which was in good agreement with the observed weight gain of ≈25–26% occurring after fluorination

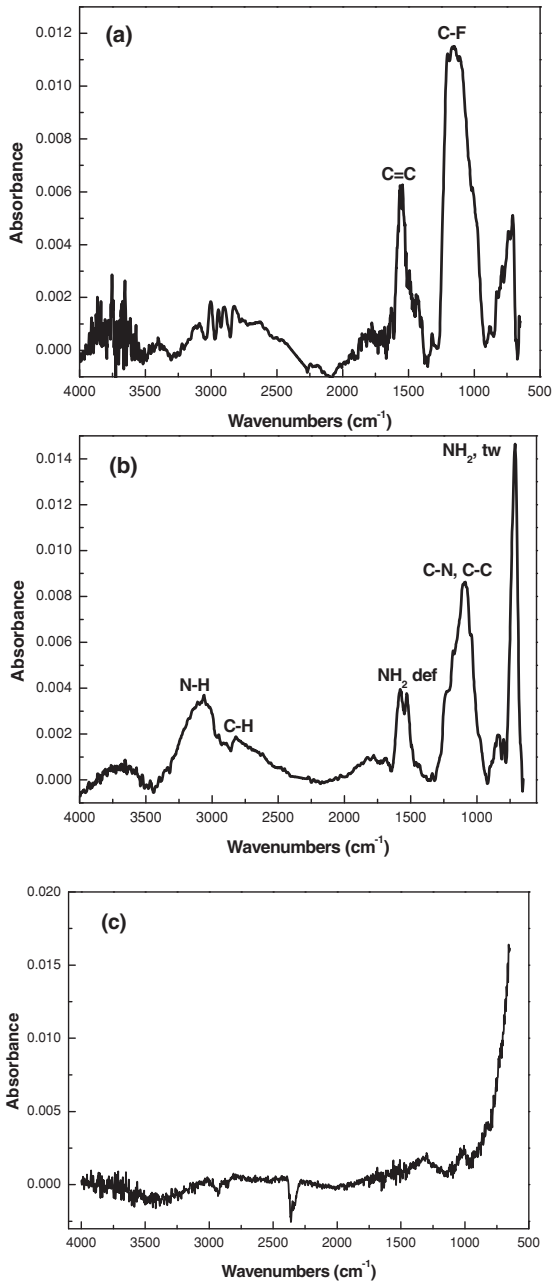

Figure 1. ATR-FTIR spectra of fluorinated CNFs (a), amino-functionalized CNFs (b), and pristine CNFs (c).

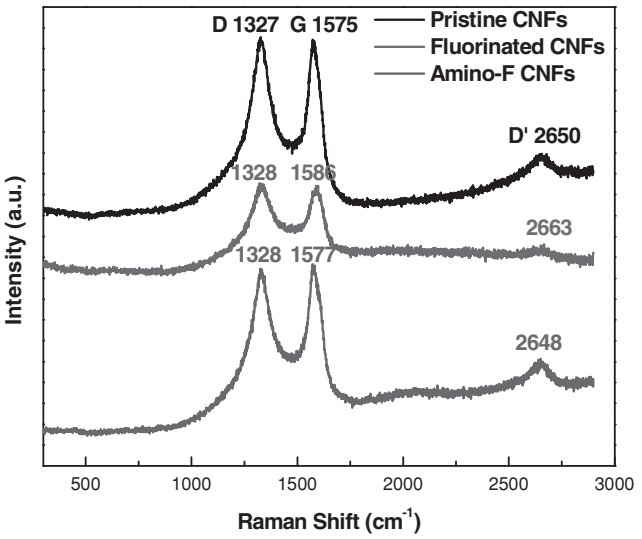

Figure 2. Raman spectra of pristine, fluorinated, and amino-functionalized CNFs.

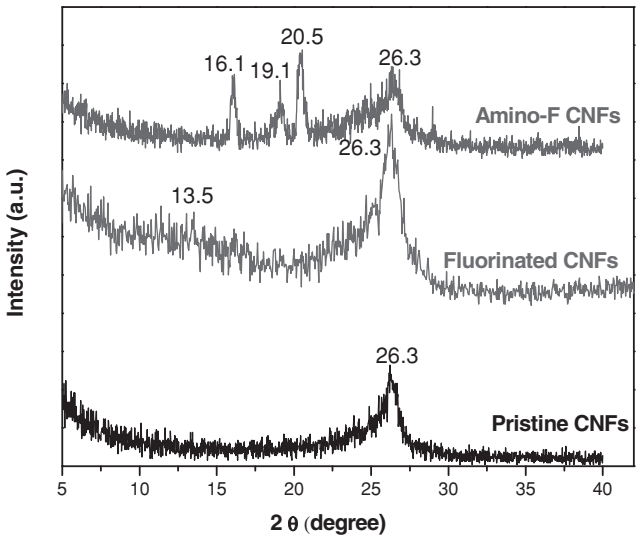

Figure 3. XRD patterns of pristine, fluorinated, and amino-functionalized CNFs.

of CNFs. In comparison, amino-functionalized CNFs exhibited weight loss of about 20% in a narrow temperature range of 180–250 °C, which was similar to carbon nanotubes that were also functionalized with ethylene diamine through reaction with fluorinated derivatives. Elemental analysis by X-ray photoelectron spectroscopy (XPS) showed atomic concentration (at%) on the surface of functionalized CNF as follows: fluorinated CNFs, C (50.8), O (4.2), F (45.0); amino-functionalized CNFs, C (70.0), N (13.3), O (7.6), F (9.1). The covalent bonding of fluorine to the CNFs was evidenced by observation of the F1s peak in the XPS spectra (not shown here) at binding energies of 687.4–687.8 eV which is typically observed for fluorine covalently bonded to carbon.[18]

Raman spectroscopy provided essential information to evaluate the bonding states of carbons in the fiber structure changed by fluorination and amination. The Raman spectra collected from the pristine, fluorinated as well as the amino-functionalized CNFs were shown here (**Figure 2**). In the spectrum of the pristine CNFs, a strong and sharp peak at 1575 cm^{-1} (G band) corresponded to the in-plane stretching vibration of the sp^2 carbon-carbon bonds within the ordered graphitic layers of fibers, while another strong peak at 1327 cm^{-1} (D band) was related to the defects in the graphene structure. A weaker peak at 2650 cm^{-1} (D′ band) reflected the boundary point K in Brillouin zone of graphite and was dependent upon the packing in three-dimensional space.[19] For the fluorinated CNFs, the Raman "red shift" in G (1575 cm^{-1} to 1586 cm^{-1}) and D′ (2650 cm^{-1} to 2663 cm^{-1}) bands occurred due to the difference in microstructure, such as the interlayer distance. Another thing worth mentioning was that the D′ shift could be due to the introduced compressive force on the fiber surface,[20] which was also evidenced by TEM images later. In comparison, the G and D′ bands shifted back to pristine fiber's positions after grafting amino functional group.

Significant changes in the structure of CNFs caused by the functionalization were detected through X-ray diffraction (XRD) measurements. As comparison of XRD patterns (**Figure 3**), the fluorination of CNFs caused the appearance of a very broad new feature in the XRD of the fluorinated CNFs centered at 2θ = 13.5°, as found by the curve-fitting analysis, in addition to a typical graphite (002) peak at 2θ = 26.32°. Based on XPS surface analysis, the outer layers of the fluorinated CNFs were built from fluorographene layers of C_1F_1 composition. According to the calculation from XRD value of interlayer distance, these layers were separated by d-spacing equal to 0.657 nm which matched the interplanar d-spacing in fluorographite $CF_{1.12}$ (0.57–0.66 nm),[21] indicating strong repulsive interactions between curved fluorographene layers in fluorinated CNFs.

XPS data also showed that although reaction of fluorinated CNFs with ethylenediamine resulted in grafting of $–NHCH_2CH_2NH_2$ groups to the surface of CNFs, complete removal of fluorine did not take place, so about 9 at% fluorine still remained bonded in the structure. Nevertheless, such defluorination of the fluorinated CNFs produced a significant decrease of interlayer spacing since stoichiometry of fluorographene layers in amino-functionalized CNFs became reduced from C_1F_1 to approximately C_5F and below, as calculated from XPS elemental analysis data. It was witnessed by complete disappearance of a low angle peak observed on the fluorinated CNFs and appearance of new sharp peaks at 2θ = 16.14, 19.1, and 20.48°, along with the peak of neat CNFs at 2θ = 26.32° (Figure 3), which corresponded to d-spacing of 0.535, 0.464, 0.433, and 0.338 nm, respectively.

2.2. The Mechanical Properties of Functionalized CNFs

With the successful functionalization of CNFs by fluorine and amino groups along with the corresponding chemical characterizations completed, quantitative in situ tensile testing method as described later was employed to investigate the mechanical consequences of such chemical treatments on individual CNFs. At least 10 samples for each type of CNFs were successfully

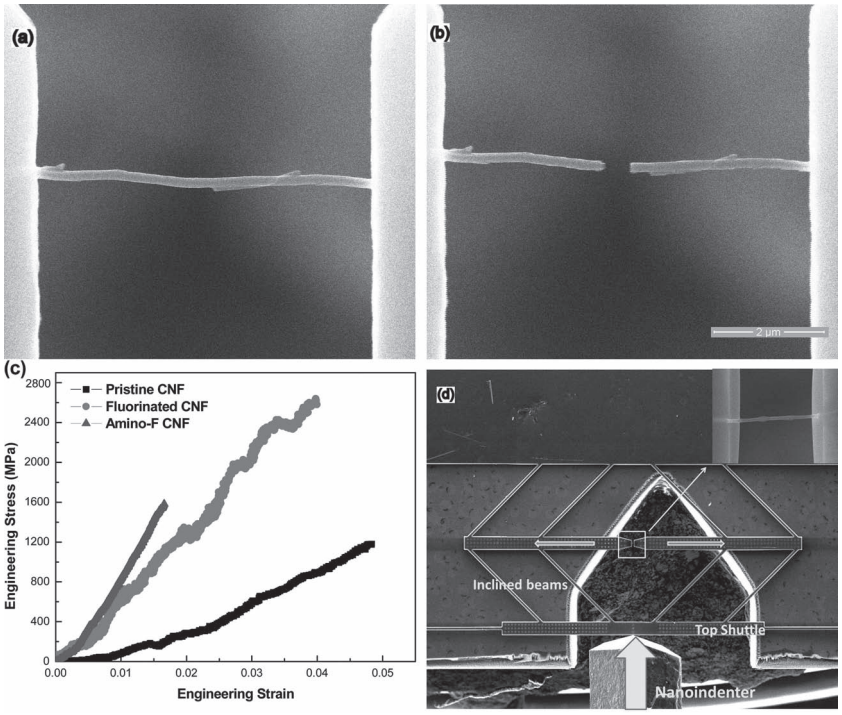

Figure 4. a,b) SEM images show a pristine CNF specimen before tension and after failure. c) Tensile test engineering stress versus strain curves for the pristine CNF specimen, the fluorinated CNF specimen, and the amino-functionalized CNF specimen. d) SEM image of the in situ tensile test platform: block arrows show the direction of movement of the indenter tip and the shuttles during the experiment. Inset: close up view of rectangle region showing a CNFs specimen across the sample stage shuttle gap.

tested and the deformation and fracture of individual CNFs were closely monitored by real time SEM imaging. A simple microfabricated device (**Figure 4**) that works in conjunction with a quantitative nanoindenter within an SEM/TEM chamber was used to perform in situ tensile tests on functionalized CNFs. Loads applied to the samples and the sample elongations were derived from the nanoindenter load and the displacement data using a simple response subtraction method and image correlation techniques.[22] The snapshots of the pristine CNFs during tension and after failure as well as the selected stress versus strain curves of three different types of CNFs (Figure 4) exhibit an initial gradual change in the fiber stiffness. It is due to the fiber waviness in its natural state after sample mounting, and the sample would need to be first pulled straight before any load application can occur. The rest of stress-strain curves show a typical linear elastic deformation behavior observed in carbon nanotubes and similar 1D nanomaterials. It is evident that the strength of fibers increased dramatically after the fluorination but dropped back to the similar level as the pristine CNFs after further partial defluorination and grafting of ethylenediamino functional groups (**Table 1**). These obtained strength values also compare favorably with the limited data available in the literature from direct measurements of individual CNFs.[12]

Due to the stochastic nature of the mechanical properties measured for CNFs, a probabilistic analysis using two parameter Weibull cumulative probability density function[23] was applied to evaluate the tensile strength of CNFs:

$$p_f(\sigma) = 1 - \exp\left(-\left(\frac{\sigma}{\sigma_0}\right)^m\right) \quad (1)$$

where σ, is the applied stress resulting in a probability of failure, $P_f(\sigma)$, m is the Weibull modulus, which provide a measure of the scatter in the strength data, and σ_0 is the material stress parameter. The Weibull parameters were computed by the method reported by Klein.[24,25] Specifically, ranking the failure stresses (σ_i) in the ascending order (i = 1, 2,…n) and assigning probabilities of failure according to $P_i = (i\text{-}0.5)/n$, where n is the number of broken specimens, are the initial task to estimate the cumulative failure probability from the available failure-stress data. Subsequently, a linear curve fitting with a logarithmic axis was performed for data collected from all three types of CNFs to obtain the corresponding Weibull parameters as listed in Table 1.

In the study of Endo et al.,[26] the majority of fiber strength values for VGCNFs diameter between 300–1000 nm are in the range of 500–1000 MPa, and the mechanical strength of VGCNFs is found to be inversely related to the diameter size. The trends proposed by them could predict the higher strengths measured in this study, in which the size of three types of CNFs ranged between 200 and 250 nm. Compared to the pristine CNFs, the other two functionalized CNFs have relatively small Weibull moduli which indicate the presence of a broader spectrum of flaws.[27] The characteristic strength of the pristine CNFs is 2.10 GPa compared to 3.05 GPa for the fluorinated CNFs, see Table 1. The negative effect of partial defluorination and further amino functional group grafting on the average CNFs strength is evidenced by the fact that the characteristic

Table 1. Weibull parameters, elastic moduli, mean strength, and strain for three types of CNFs.

Nanofiber sample	Sample diameter [nm]	Weibull modulus, m	Characteristic strength, σ_0 [GPa]	Elastic modulus, E [GPa]	Average strength [GPa]	Average strain
Pristine CNFs	210 ± 30	3.39	2.10	25.8 ± 3.3	1.89 ± 0.66	0.063 ± 0.021
Fluorinated CNFs	221 ± 25	2.83	3.05	45.8 ± 10.2	2.67 ± 0.94	0.057 ± 0.015
Amino-F CNFs	215 ± 38	3.13	1.94	31.6 ± 13.8	1.75 ± 0.68	0.053 ± 0.013

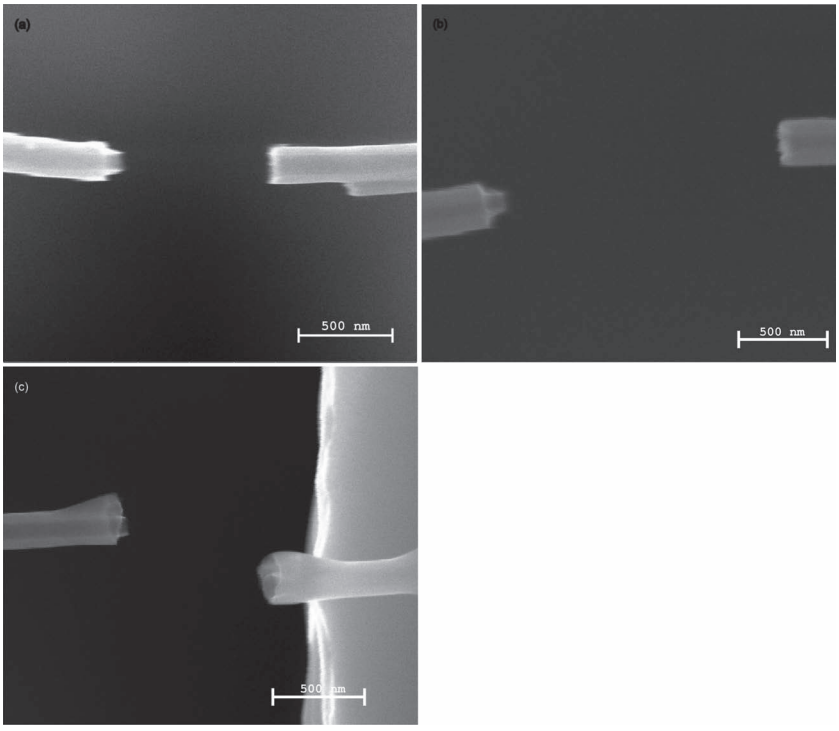

Figure 5. Representative SEM images of ruptured surfaces of a) pristine CNFs, b) fluorinated CNFs, and c) amino-functionalized CNFs.

strength decreases significantly to 1.94 GPa, even lower than that of the pristine CNFs. The great decrease of characteristic strength reveals a dramatic increase in the average size of the catastrophic flaws after amnino functionalization. On the other hand, the greater variability of the strength and the smaller Weibull modulus for the fluorinated CNFs suggest that the fluorination increases the randomness in the distribution and variability of flaw size. Finally, the elastic modulus measured for different CNFs samples follow the similar trend. These results are comparable with the elastic modulus of amorphous and hollow CNFs based probes calculated to be 42 GPa.[11]

2.3. Fracture Surfaces

Next, fracture modes of the CNFs were studied by high resolution SEM imaging of the fracture surfaces. The close up views of fracture specimens of the pristine (**Figure 5**a), fluorinated (Figure 5b) and amino-functionalized (Figure 5c) CNFs demonstrate that all three types of fiber failed in the similar cup-and-cone fashion reported earlier.[12,28,29] Suzuki[28] observed the cup-shaped morphology in the fractured ends of the CNFs, and he claimed that the relatively weak interlayer bonding was responsible for the observed breakdown. Brown et al.[29] applied about 5% strain on fibers made of CNTs within amorphous carbon resulted in a permanent damage to its outer shells, giving rise to the plastic deformation until the outer shell eventually fractured and the inner layers nearly pulled out. In this study, due to the turbostratic nature of CNFs walls, it is hypothesized that fracture begins in the outer layers where carbon structure is more disordered. Therefore, failure could initiate in the outer fiber layers with subsequent sliding of the inner graphitic layers, leading to the complete final fracture of the whole fiber.

The fine details of the cone structures in the pristine, fluorinated and amino-functionalized CNFs were further revealed by HRTEM images (**Figure 6**). It was found that the diameter of the hollow core remained unchanged in the cone section for the pristine (Figure 6a) and amino-functionalized (Figure 6c) CNFs, compared to the fiber section without broken out layers further away from the fracture surface. Surprisingly, such well-expected morphology changed drastically in the fluorinated CNFs, where the diameter of the hollow core in the cone section expanded almost 5 times as compared to the hollow core diameter in the fiber section away from the fracture surface (Figure 6b). Also apparent from the insets of these HRTEM images, the inner carbon layers of all CNFs appeared to be more ordered as clearly shown in the magnified view of layer structures in the cone sections (Figure 6 insets).

In order to better understand these intriguing fracture processes in CNFs with different chemical functionalization treatments, we need to first carefully evaluate the resulting structures of these functionalized CNFs. A simple schematic illustration of the complete fluorination and amination processes of CNFs is shown in (**Scheme 1**) to facilitate our understandings. For better illustration of the fluorinated CNFs structure, the distance between the fluorine atoms and fiber surface are exaggerated while the bold segments represent the fluorocarbons layers. During the fluorination process, previous XPS studies have shown that most of the fluorine atoms are expected to bond covalently on CNFs' outer layers. It should be noted that the hollow core can shrink due to the repulsive interaction of thicker fluorocarbons layers which is mostly directed inward. Such phenomenon has already been reported by Liu et al.[30] where a similar fluorination method was used for the treatment of carbon nano-onions. It was found that the fluorination process disrupted the integrity of the graphene layers in the onions by formation of fluorographene segments which compressed their interior structure, while the subsequent de-fluorination of carbon nano-onions by hydrazine treatment resulted in remarkable "healing" of broken graphene layers which recovered the original inner structure. In our case, it is believed that the diameter of the hollow core has been mostly recovered after defluorination and grafting of ethylenediamion groups predominantly to the CNFs surfaces as shown in Scheme 1.

Therefore, a possible scenario was proposed that the compressive force could be introduced on CNFs surfaces during the fluorination owing to the repulsive interactions of outer fluorocarbon layers, which could not only lead to a smaller hollow core diameter but also positively improve the nominal mechanical strength of the fluorinated CNFs. In fact, such improvements

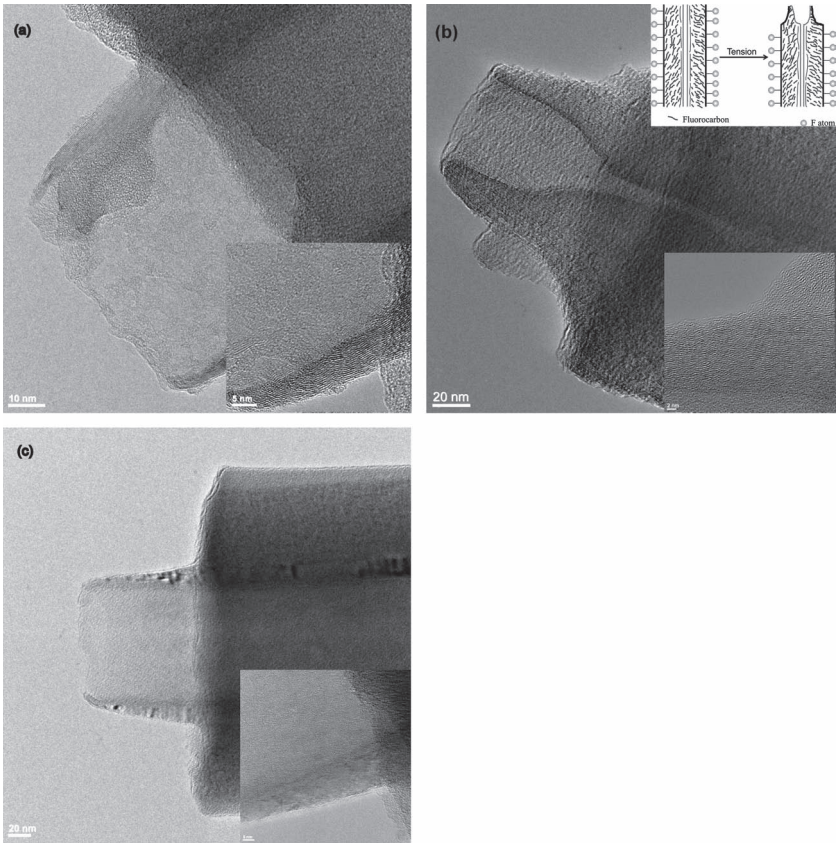

Figure 6. a) HRTEM image of the pristine CNF fracture surface. The diameter of the hollow core was kept the same in both cone and intact fiber sections after failure; the inset in bottom right corner shows more ordered inner layers of the pristine CNF. b) HRTEM images of the fluorinated CNF fracture surface clearly showing the dramatic change of hollow core diameter from the cone to intact fiber section. The top inset shows a schematic illustration of the hollow core diameter change before and after fluorinated CNF fracture and the bottom inset shows more ordered inner layers of the fluorinated CNF. c) HRTEM images of the amino-functionalized CNF fracture surface. The diameter of hollow core was kept the same after failure in both cone and intact fiber sections; the inset shows more ordered inner layers of the amino-functionalized CNF.

were indeed observed in both average strength and Weibull characteristic strength values of fluorinated CNFs (Table 1). When the failure initiated at the less ordered outer layers as discussed earlier and then grew inward, the cup-and-cone type of fracture would develop facilitated by the relative sliding of more ordered inner layers with respect to the outer layers. Once the fluorinated CNFs fractured, the break-off of the outer layers in the cone side of the fracture surface would release the compressive force causing an abrupt hollow core expansion as observed in Figure 6b. In the subsequent amino-functionalization procedures, the fluorination induced compressive force on CNFs surfaces was mostly released due to the de-fluorination process while further grafting of amino functional groups had minimum impact on CNFs hollow core size, promoting the recovery of hollow core size for amino-functionalized CNFs. This change was reflected by the similar fracture surface features (Figure 6a,c) and the average strength in the similar level (Table 1), although the strength of amino-functionalized CNFs was slightly lower due to the inevitable disruption of the CNFs surfaces and introduction of additional defects during the functionalization procedures.

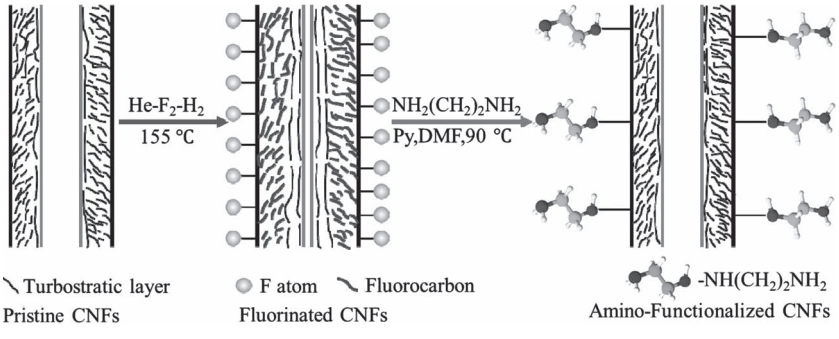

Scheme 1. Schematic illustration of the complete functionalization process for CNFs. Note that the hollow core shrinks after fluorination and recovers after defluorination associated with amino-functionalization.

3. Conclusions

We have successfully demonstrated the fluorination and amination of CNFs for their potential applications in composite materials. The mechanical properties of individual pristine, fluorinated and amino-functionalized CNFs have been quantified by in situ tensile experiments inside a SEM sample chamber. Post-mortem SEM and HRTEM images of the fracture surface reveal that all types of CNFs samples fail in the similar cup-and-cone fashion. The pristine CNFs have an average mechanical strength of 1.89 GPa and a Weibull characteristic strength of 2.10 GPa. Fluorination treatment increases the nominal mechanical strength of CNFs by ≈30–40% through possible introduction of compressive force on CNFs surfaces, which is supported by the observed discrepancy in diameters of the hollow core between the cone section and the intact fiber section away from the fracture surfaces of the ruptured CNFs. However, further amino functional group grafting on CNFs reduces their mechanical strength. The relative small Weibull moduli of the fluorinated and amino-functionalized CNFs as well as their increased standard deviation of strength indicate a broader flaw population, compared to the pristine CNFs, which are attributed to the generated defects during functionalization procedures. The insights provide in this work could certainly benefit an in-depth understanding of mechanical properties of these

important nanoscale reinforcing entities and their subsequent integration into a variety of nanocomposites with superior mechanical performances.

4. Experimental Section

The method for the fluorination of carbon nanotubes (CNTs) described elsewhere[15] was used here. In a typical fluorination process, (1.75 g) of commercially available pristine CNFs (Pyrograf-III, batch PR-19-XT-PS from PPI, Cedarville, Ohio) was loaded into a custom-built fluorination apparatus. The chamber was purged with the flow of helium while the temperature was ramped to 155 °C. At this temperature, the fluorination was carried out for 16 hours by passing a 10% fluorine-90% helium gas mixture over the CNFs in the chamber. The unreacted F_2 gas was absorbed into a trap containing aqueous solution of KOH. After cooling to the room temperature, (2.16 g) of the fluorinated CNFs were produced, which resulted in the covalent addition of about 25 wt% of fluorine on CNFs surface.

Amination of CNFs was carried out by analogy with the amino functionalization of fluorinated CNTs.[16,17] (2 g) of fluorinated CNFs, (20 ml) of ethylenediamine, and (200 ml) of DMF were placed into a 500 ml three-neck flask, equipped with the thermometer and condenser, then 1 ml of pyridine was added. The mixture was stirred overnight at 90 °C under nitrogen. After cooling down to the room temperature, the mixture was filtered through a 0.22 μm Teflon membrane (Millipore, Billerica, MA) and the residue on the membrane washed with ethyl alcohol, then dried overnight at 70 °C in vacuum oven. As the result, (1.85 g) of amino-functionalized CNFs was prepared.

In order to confirm the effective functionalization by fluorination and subsequent amination, and also to evaluate the concentration of the fluorine and amino groups on CNFs surfaces, the bonding nature of carbon in functionalized CNFs, and finally the effects of fluorination and amination on CNFs structures, a series of careful investigations utilizing ATR-FTIR, XPS, Raman spectroscopy, TGA, and XRD were conducted. ATR-FTIR spectra were collected using a Ge crystal attachment at Nicolet 4700 spectrometer. XPS measurements were made using a PHI 5700 with Al Kα X-rays (1486.6 eV) at a maximum pressure of 4×10^{-8} torr. Raman spectroscopic measurements were collected with a Renishaw 1000 microraman system operating with a 532 nm laser source. TGA was performed in flowing air on a TA Instruments Q500 by heating the sample from 25 to 1000 °C using a ramp rate of 10 °C/min. XRD patterns of powder samples deposited on a zero-background quartz crystal plate were collected on a Siemens D5000 using a Cu Kα source ($\lambda = 0.154$ nm).

The details about the microdevice fabrication using standard photolithography techniques were discussed earlier.[31] In conjunction with a quantitative nanoindenter within an SEM/TEM chamber, the micro-device was employed to perform in situ tensile tests on 1D nanoscale specimens.[22,31–33] A thin fresh layer of epoxy (HARDMAN Water-Clear Epoxy) was first deposited on a small portion of sample stage shuttle. A droplet from the sonicated suspension of the CNFs in toluene was dropped onto a Si wafer coated with a 5 nm thick layer of titanium. Individual nanofiber of 200–250 nm diameters was subsequently picked up and placed across the shuttles using micromanipulators housed within a probe station (The micromanipulator Co., Carson City, NV) under an optical microscope.

Uniaxial tensile experiments of individual pristine, fluorinated and amino-functionalized CNFs were conducted within a SEM (FEI Quanta 400 high resolution field emission scanning electron microscope, FEI Company, Hillsboro, Oregon) equipped with an InSEM Indenter (AGILENT Technologies, Oak Ridge, Tennessee) system. A blunt Berkovich nanoindenter tip was used to apply load at a displacement rate of ≈20 nm/s. The maximum load applied to the device ranged from 0.3 mN to 0.5 mN. After each experiment, both ends of the ruptured CNFs were imaged by SEM at higher magnification to identify the fracture mode. Since it was not always possible to accurately measure the inner radius of the hollow CNFs, the analysis employs solely the outer CNFs diameter to estimate the nominal fiber strength. Due to the relative low stiffness of epoxy clamps, the displacement of the deformable epoxy clamps during testing need to be carefully considered. To ensure the accuracy of displacement measurement, a digital image correlation method was utilized, and all results reported in this work have been corrected by this technique. A selected number of ruptured samples were further analyzed post-mortem by a HRTEM (JEM 2100F HR-TEM) to closely examine the fine details of fracture surface features.

Acknowledgements

The authors acknowledge support from the National Science Foundation grant NSF CMMI 0800896, the Welch Foundation grant C-1716 and Air Force Research Laboratory grant AFRL FA8650-07-2-5061. V.K. acknowledges PipeWrap, LLC, for partial support.

Received: February 29, 2012
Revised: May 9, 2012
Published online: June 5, 2012

[1] E. Fitzer, *Carbon Fibers and Their Composites*, Springer, New York **1985**.
[2] J. L. Figueiredo, *Carbon Fibers, Filament and Composites*, Kluwer, Dordrecht, The Netherlands **1990**.
[3] P. E. Morgan, *Carbon Fibers and Their Composites*, CRC Press, Boca Raton, FL **2005**.
[4] B. Eksioglu, A. Nadarajah, *Carbon* **2006**, *44*, 360.
[5] J. G. Lawrence, L. M. Berhan, A. Nadarajah, *J. Nanopart. Res.* **2008**, *10*, 1155.
[6] C. Wei, *Appl. Phys. Lett.* **2004**, *85*, 2208.
[7] G.-T. Kim, G. Gu, U. Waizmann, S. Roth, *Appl. Phys. Lett.* **2002**, *80*, 1815.
[8] J. G. Lawrence, L. M. Berhan, A. Nadarajah, *ACS Nano* **2008**, *2*, 1230.
[9] H. Zhang, J. Tang, P. Zhu, J. Ma, L.-C. Qin, *Chem. Phys. Lett.* **2009**, *478*, 230.
[10] E. Zussman, X. Chen, W. Ding, L. Calabri, D. A. Dikin, J. P. Quintana, R. S. Ruoff, *Carbon* **2005**, *43*, 2175.
[11] K. Inaba, K. Saida, P. Ghosh, K. Matsubara, M. Subramanian, A. Hayashi, Y. Hayashi, M. Tanemura, M. Kitazawa, R. Ohta, *Carbon* **2011**, *49*, 4191.
[12] T. Ozkan, M. Naraghi, I. Chasiotis, *Carbon* **2010**, *48*, 239.
[13] S. N. Arshad, M. Naraghi, I. Chasiotis, *Carbon* **2011**, *49*, 1710.
[14] Z. Zhou, C. Lai, L. Zhang, Y. Qian, H. Hou, D. H. Reneker, H. Fong, *Polymer* **2009**, *50*, 2999.
[15] V. N. Khabashesku, W. E. Billups, J. L. Margrave, *Acc. Chem. Res.* **2002**, *35*, 1087.
[16] V. N. Khabashesku, M. X. Pulikkathara, *Mendeleev Commun.* **2006**, *16*, 61.
[17] V. N. Khabashesku, *Russ. Chem. Rev.* **2011**, *80*, 705.
[18] T. Nakajima, *Fluorine-Carbon and Fluoride-Carbon Materials*, Marcel-Dekker, New York **1995**.
[19] C. Pan, Q. Bao, *J. Mater. Sci. Lett.* **2002**, *21*, 1927.
[20] L. S. Schadler, S. C. Giannaris, P. M. Ajayan, *Appl. Phys. Lett.* **1998**, *73*, 3842.
[21] R. J. Lagow, R. B. Badachhape, J. L. Wood, J. L. Margrave, *J. Chem. Soc., Dalton Trans.* **1974**, *12*, 1268.
[22] Y. Lu, Y. Ganesan, J. Lou, *Exp. Mech.* **2010**, *50*, 47.
[23] A. Hallian, *J. Quality Technol.* **1993**, *25*, 85.
[24] ASTM, *ASTM Designation C1239*, (Ed: Int'l Library Service 5), Provo, UT **1995**.

[25] C. A. Klein, *Opt. Eng.* **2009**, *48*, 113401.
[26] M. Endo, Y. A. Kim, T. Hayashi, K. Nishimura, T. Matusita, K. Miyashita, M. S. Dresselhaus, *Carbon* **2001**, *39*, 1287.
[27] P. Mangonon, *The principles of materials selection for engineering design*, 1st ed, PrenticeHall, Upper Saddle River, NJ **1999**.
[28] M. Suzuki, *J. Appl. Phys.* **2007**, *101*, 114307.
[29] J. J. Brown, J. W. Suk, G. Singh, A. I. Baca, D. A. Dikin, R. S. Ruoff, V. M. Bright, *Sens. Actuators A* **2009**, *155*, 1.
[30] Y. Liu, R. L. Vander Wal, V. N. Khabashesku, *Chem. Mat.* **2007**, *19*, 778.
[31] Y. Ganesan, L. Yang, P. Cheng, L. Hao, R. Ballarini, L. Jun, *J. Microelectromech. Sys.* **2010**, *19*, 675.
[32] Y. Ganesan, C. Peng, Y. Lu, L. Ci, A. Srivastava, P. M. Ajayan, J. Lou, *ACS Nano* **2010**, *4*, 7637.
[33] Y. Lu, J. Y. Huang, C. Wang, S. Sun, J. Lou, *Nat. Nanotechnol.* **2010**, *5*, 218.